J. Fluid Mech. (2010), *vol.* 659, *pp.* 516–539.
doi:10.1017/S0022112010002715

The intermediate wake of a body of revolution at high Reynolds numbers

JUAN M. JIMÉNEZ†, M. HULTMARK AND A. J. SMITS

Department of Mechanical and Aerospace Engineering, Princeton University, Princeton, NJ 08544, USA

(Received 13 January 2010; revised 6 May 2010; accepted 6 May 2010; first published online 27 July 2010)

Results are presented on the flow field downstream of a body of revolution for Reynolds numbers based on a model length ranging from 1.1×10^6 to 67×10^6. The maximum Reynolds number is more than an order of magnitude larger than that obtained in previous laboratory wake studies. Measurements are taken in the intermediate wake at locations 3, 6, 9, 12 and 15 diameters downstream from the stern in the midline plane. The model is based on an idealized submarine shape (DARPA SUBOFF), and it is mounted in a wind tunnel on a support shaped like a semi-infinite sail. The mean velocity distributions on the side opposite the support demonstrate self-similarity at all locations and Reynolds numbers, whereas the mean velocity distribution on the side of the support displays significant effects of the support wake. None of the Reynolds stress distributions of the flow attain self-similarity, and for all except the lowest Reynolds number, the support introduces a significant asymmetry into the wake which results in a decrease in the radial and streamwise turbulence intensities on the support side. The distributions continue to evolve with downstream position and Reynolds number, although a slow approach to the expected asymptotic behaviour is observed with increasing distance downstream.

Key words: separated flows, shear layer turbulence

1. Introduction

Turbulent wakes are one of the least studied flows, mostly due to their long development length and the difficulty in measuring low-level turbulent intensities in the far wake. Most of the previous works have focused on the behaviour of plane wakes, such as those produced by circular cylinders, flat plates and airfoils (Goldstein 1948; Townsend 1956; Wygnanski, Champagne & Marasli 1986; Oertel 1990), and most wake measurements have been performed at low to moderate Reynolds numbers. The behaviour at high Reynolds numbers typical of large-scale vehicles is still largely unexplored.

In a major contribution that has shaped much of the research in this area, Townsend (1956) proposed that the far wake should approach a state of self-similarity and become Reynolds-number-independent. In the far wake, the flow is in a state of

† Present address: Institute for Medicine and Engineering, University of Pennsylvania, Philadelphia, PA 19104, USA. Email address for correspondence: jjimenez@upenn.edu

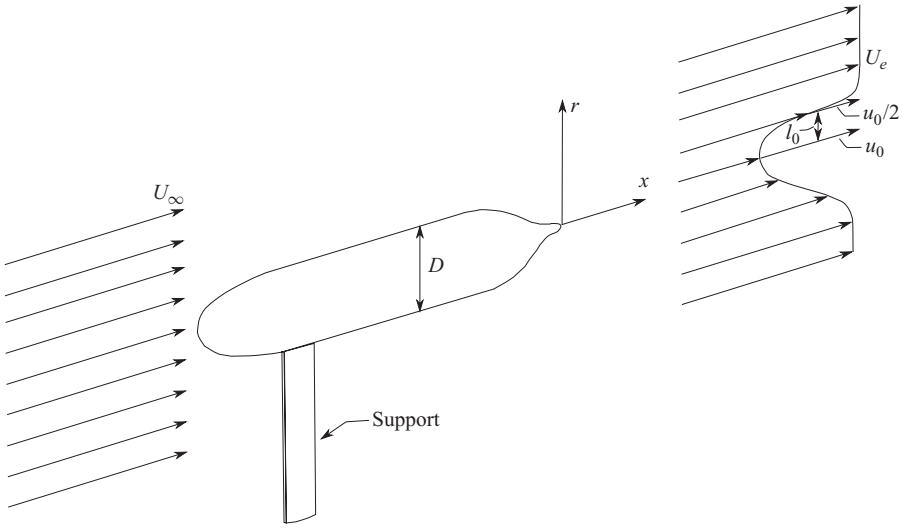

FIGURE 1. Wake flow behind an axisymmetric body with nomenclature.

moving equilibrium where the mean and turbulent flow quantities can be determined exclusively by a local velocity scale u_0, the maximum velocity deficit and a length scale l_0, the distance from the centreline to the point where the velocity deficit equals $u_0/2$ (see figure 1).

Townsend (1956) further proposed that rapid attainment of self-similarity requires relatively low turbulence production rates within the separated zone near the body. In general, the wakes behind streamlined bodies of revolution appear to become established more quickly than for axisymmetric bluff bodies such as disks (Carmody 1964; Chevray 1968; Sirviente & Patel 1999; Johansson & George 2006*a*,*b*). Chevray (1968) reported that the 6:1 prolate spheroid at a Reynolds number based on the length of 2.75×10^6 produced a small separated flow zone extending about $0.12D$ upstream and $0.10D$ downstream of the stern. The mean velocity distributions in the wake were self-similar for $x/D > 3$, where x is measured in the streamwise direction downstream from the stern, and D is the maximum diameter of the model. In contrast, measurements at a Reynolds number of 7×10^4 based on diameter and free-stream velocity in the wake of a circular disk, which generates a region of separated flow that is several diameters long, showed that the mean velocity attained self-similarity only for $x/D \geqslant 15$ (Carmody 1964). However, at a Reynolds number of 1.93×10^5 the mean velocity in the wake of disks and cups attained self-similarity for $x/D \geqslant 3$, although the wake of the disk took longer to recover (Desabrais & Johari 2006). Studies by Sirviente & Patel (1999) compared the effects of stern shape on wake development for two similar axisymmetric bodies, one with an intact stern and the other with a truncated stern, and found that the flow over the truncated model separated earlier than the intact one, resulting in an initially larger wake width and a faster attainment of self-similarity. Wygnanski *et al.* (1986) also showed that the approach to self-similarity in plane wakes depends strongly on the nature of the wake generator. Results by Symes & Fink (1977) on the wakes of circular cylinders oriented normal to the flow direction suggest that the wake development also depends, to a large extent, on the ratio of the length scale of the external turbulence to that of the wake.

More recent experiments in the wake generated by a circular disk for $10 \leqslant x/D \leqslant 150$ at a Reynolds number of 26.4×10^4 showed that the mean velocity was self-similar at all stations downstream, but the turbulence distributions did not become self-similar until $x/D = 30$ (Johansson & George 2006*a*,*b*). We define this region as the intermediate wake, that is, where the mean flow is self-similar, but the turbulence has not yet reached that state. The extent of the intermediate wake will depend on the wake generator, the free-stream turbulence level and the streamwise pressure gradient, among other parameters.

The presence of the support can obviously alter the flow field in the wake of the body of interest. The wake studies by Gear (1965) on a 6:1 prolate spheroid showed a marked influence by the support system on the wake development, leading Chevray (1968) to use two sets of four steel wires to suspend the model in an effort to minimize the support interference. Huang *et al.* (1992) found that the wake of a body of revolution supported by streamlined struts displayed an altered local flow field, and most other wake studies have employed wires as a means of suspension to minimize flow disturbances (Merz, Yi & Przirembel 1985; Higuchi & Kubota 1990; Sirviente & Patel 1999; Johansson & George 2006*a*,*b*).

The present study addresses the wake of a body of revolution over a wide range of Reynolds numbers, including the effects of the support. The model geometry is based on the Defense Advance Research Projects Agency (DARPA) SUBOFF geometry as described by Groves, Huang & Chang (1989). The flow over this model has been studied by various investigators, but few have focused on the wake. Huang *et al.* (1992) conducted experiments on the flow over the body at a Reynolds number based on the length of 12×10^6, and also performed extensive numerical computations for this configuration. Their measurements did not extend into the wake, but Jiménez, Reynolds & Smits (2010) surveyed the early intermediate wake of an appended SUBOFF body configuration with fins on the stern for a range of Reynolds numbers up to 1.8×10^6. Sheng, Taylor & Whitfield (1995) and Hosder (2001) studied the effect of yaw, and Sheng *et al.* (1995) also conducted numerical computations for configurations with fins at a Reynolds number of 12×10^6 in order to compare them to the experimental results of Huang *et al.* (1992). Several other computational analyses have been conducted to validate computational fluid dynamics (CFD) codes, help understand the complex flow about a submarine model with different configurations and describe the fluid motions about a submarine conducting manoeuvres (Sung *et al.* 1993; Bull 1996; McDonald & Whitfield 1996; Arabshahi *et al.* 1998; Alin, Berglund & Fureby 2000).

Here, we study the approach to self-similarity in the intermediate wake region ($x/D \leqslant 15$). This is one of a very small number of experiments on body-of-revolution wakes, and it spans a large range of Reynolds numbers, from $Re_L = 1.1 \times 10^6$ to 67×10^6, where Re_L is the Reynolds number based on the model length L and the free-stream velocity U_∞. The highest Reynolds number is at least an order of magnitude larger than any previous wake study, regardless of how the wake was generated. The present experiments also examine the influence of the support on the development of the wake. The support creates a junction flow with the hull where the boundary layer separates from the hull due to an adverse pressure gradient upstream of the support, and horseshoe vortices are formed and stretched downstream by the fluid flowing around the support (Simpson 2001). Given that the support has the same cross-section as the sail of the SUBOFF model, the present experiments should provide insight into the effects of the sail of a submarine, and more generally, any streamlined support system or appendage, on the development of the wake.

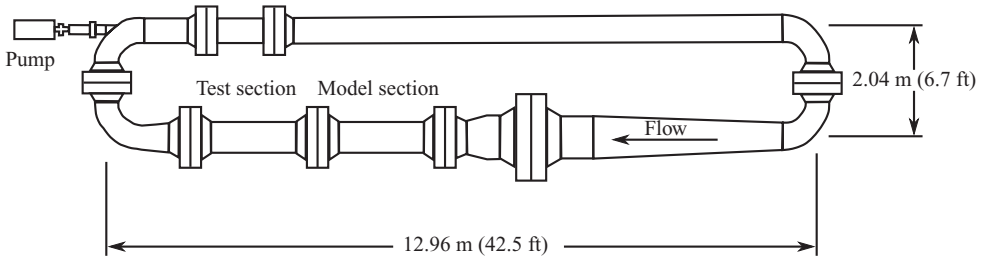

FIGURE 2. The Princeton High Reynolds Number Test Facility.

2. Experimental arrangements

The model was tested in the High Reynolds Number Test Facility (HRTF), a closed-loop wind tunnel in the gas dynamics laboratory in Princeton University. This facility achieves a wide range of Reynolds numbers by using compressed air as a working fluid, with pressures up to 238 atm. A three-phase 149 kW motor drives the impeller allowing velocities up to about 10 $\mathrm{m\,s^{-1}}$. A honeycomb, a mesh, two screens and a circular 2.2:1 contraction section are used to minimize the free-stream turbulence levels, which range from 0.3 % at the lowest Reynolds number to 1.1 % at the highest Reynolds number. The HRTF has two working sections each 2.44 m long with a 0.61 m outer diameter and 0.49 m inner diameter. The model was installed in the upstream section, and the wake measurements were conducted in the downstream section (see figure 2). Further details of the HRTF and the experiments described here are given by Jiménez (2007).

The wake was generated by a 1/120 DARPA SUBOFF model (Groves *et al.* 1989), with an overall length $L = 0.87$ m and a maximum diameter $D = 0.102$ m. The support cross-section corresponds to that of the sail cross-section as specified by the SUBOFF geometry. The combined blockage due to the model and support was about 5.7 %. No other appendages were used. The boundary layer was tripped about $0.75D$ downstream of the model nose with a 0.51 mm diameter trip wire. To measure the surface pressure, 45 pressure taps with inner diameters of 1.08 mm were installed in the model. The model was aligned parallel to the tunnel wall within 0.05° and verified by comparing the differential pressures over the straight portion of the body along each side of the model, which were found to be within 2.3 % of each other.

The wake was examined at Reynolds numbers of 1.1×10^6, 12×10^6, 25×10^6, 50×10^6 and 67×10^6, although the surface pressure measurements were conducted only at the three lower Reynolds numbers. To attain this range of Reynolds numbers, the tunnel static pressure was varied between 5 and 218 atmospheres. The air temperature inside the tunnel was measured using a platinum resistance temperature probe (Omega Engineering, Inc.; Stamford, CT). The pressure was monitored using three different PX303 Omega pressure transducers with full-scale pressure ranges of 50, 500 and 4000 psig (0.345, 3.35 and 27.6 MPa). One United Sensor USNH-A-368 Pitot-static tube was mounted on the traversing unit in order to calibrate the crossed-wire sensor, and another, located $14.75D$ upstream of the model, was used to determine the free-stream velocity. The Pitot-static dynamic pressures were measured using one of two Validyne DP15 pressure transducers (Validyne Engineering Corporation; Northridge, CA) with 0.86 and 22.1 kPa ranges, respectively, depending on the Reynolds number. The same transducers were used for the surface pressure measurements, which were sampled at 30 kHz for 10 s for each pressure tap.

The measurements were conducted in the midline plane of the wake, which coincides with the streamwise plane along the centre of the model and support. The traversing system could position the probes anywhere within a cylindrical volume defined by $0 \leqslant x/D \leqslant 16$, $-1.3 \leqslant r/D \leqslant 1.3$ and $0^\circ \leqslant \theta < 360^\circ$, and the probes could be pitched $\pm 15^\circ$ for calibration purposes. The flow blockage due to the traversing assembly, which is always located downstream of the stern, was about 2.3 %.

3. Hot-wire methods

To measure the streamwise and radial velocity components, a Dantec 55P51 crossed-wire probe was used, with tungsten wires of diameter $d = 5\,\mu\text{m}$ and lengths $l \approx 1\,\text{mm}$, powered by a Dantec Streamware constant temperature anemometer. The frequency response of the wires exceeded 70 kHz for all cases. The hot-wire signals were sampled at 20 kHz for 30 s at each point in the profile and low-pass filtered at 10 kHz. For all profiles, the measurement points were separated by 3.81 mm in the radial direction. Temperature increases of 0.05 °C, 0.15 °C, 0.9 °C, 2.5 °C and 10 °C were observed during the acquisition of a given velocity profile for the five Reynolds numbers studied. To account for changes in the fluid temperature, the hot-wire data were corrected according to the procedure described by Hultmark & Smits (2010). The crossed wires were calibrated for the streamwise and radial sensitivities before and after every profile, using the methods described below.

3.1. *Velocity calibration*

It was assumed that the convective heat transfer follows the cosine cooling law. That is, the crossflow sensitivity is represented by an 'effective' cooling velocity U_c given by $U_c = u\cos\phi$, where ϕ is the effective cooling angle that needs to be found by calibration.

The cooling velocities are related to the instantaneous velocities by

$$U_{c1} = (\overline{u} + u')\cos\phi_1 + (\overline{v} + v')\sin\phi_1, \tag{3.1}$$

$$U_{c2} = (\overline{u} + u')\cos\phi_2 - (\overline{v} + v')\sin\phi_2, \tag{3.2}$$

where the subscripts 1 and 2 refer to the two wires of a crossed-wire probe. The mean streamwise and radial velocity components are denoted by $\overline{u}$ and $\overline{v}$, respectively, with corresponding instantaneous velocity fluctuations, u' and v'. It is assumed that the characteristic cooling angles are independent of Reynolds number, so that (3.1) and (3.2) can be written as

$$\frac{U_{c1}}{\cos\phi_1} = \overline{u} + u' + (\overline{v} + v')\tan\phi_1 = f(E_1, \phi_1), \tag{3.3}$$

$$\frac{U_{c2}}{\cos\phi_2} = \overline{u} + u' - (\overline{v} + v')\tan\phi_2 = g(E_2, \phi_2), \tag{3.4}$$

where E is the anemometer output voltage output. Because ϕ_1 and ϕ_2 will not change for a given set of crossed wires, the calibration functions f and g depend only on E. To find f and g, we follow Perry (1982) and use fourth-order polynomials:

$$f = A_0 + A_1E_1 + A_2E_1^2 + A_3E_1^3 + A_4E_1^4, \tag{3.5}$$

$$g = B_0 + B_1E_2 + B_2E_2^2 + B_3E_2^3 + B_4E_2^4. \tag{3.6}$$

Taking the time average of (3.5) and (3.6) yields

$$\overline{f} = \overline{u} = A_0 + A_1\overline{E_1} + A_2\overline{E_1^2} + A_3\overline{E_1^3} + A_4\overline{E_1^4}, \tag{3.7}$$

$$\overline{g} = \overline{u} = B_0 + B_1\overline{E_2} + B_2\overline{E_2^2} + B_3\overline{E_2^3} + B_4\overline{E_2^4}. \tag{3.8}$$

The calibration for the streamwise velocity component requires finding the coefficients in (3.7) and (3.8). For the experiments presented here, this is done with the hot-wire probe outside the wake where $\overline{v} = 0$.

3.2. *Angle calibration*

The angle calibration method used here is an adaptation of the method proposed by Bradshaw (1971), where it is assumed that tilting the probe by an angle η changes the effective cooling angles by the same amount. Thus, for hot wires 1 and 2 with $\overline{v} = 0$,

$$\cos\eta + \tan\phi_1 \sin\eta = \frac{\overline{f}}{\overline{u}}, \tag{3.9}$$

$$\cos\eta - \tan\phi_2 \sin\eta = \frac{\overline{g}}{\overline{u}}. \tag{3.10}$$

To find ϕ_1 and ϕ_2, (3.9) and (3.10) are fitted to the calibration data obtained over the range $\pm 15°$. Note that the sign convention is such that tilting the probe by a positive value of η decreases ϕ_1 while it increases ϕ_2. The values of $\overline{u} + u'$ and $\overline{v} + v'$ are then found using (3.3) and (3.4) as follows:

$$\overline{u} + u' = \frac{f\tan\phi_2 + g\tan\phi_1}{\tan\phi_1 + \tan\phi_2}, \tag{3.11}$$

$$\overline{v} + v' = \frac{f - g}{\tan\phi_1 + \tan\phi_2}. \tag{3.12}$$

3.3. *Error estimates*

The accuracy of the temperature reading of the working fluid was about $\pm 0.5°$C. This, together with 0.25 % accuracy in the tunnel static pressure measurement, gives an uncertainty in the dynamic viscosity, μ, and density, ρ, of about ± 1.5 % and ± 0.4 %, respectively.

The velocity and turbulence intensity uncertainties were determined by calculating the quadrature sum of the propagated errors of the density calculation, pressure transducers and the largest velocity difference between the initial and final calibrations (Yavuzkurt 1984). The uncertainties were at most 0.73 %, 2.13 % and 6.58 % for the mean velocity, and the streamwise and radial turbulence intensities, respectively. The effective linear displacement resolution in the traverse was ± 0.4 μm in the radial plane and ± 6.4 μm in the streamwise direction.

Errors could also arise when measuring with crossed wires in shear layers due to the finite sensor volume. Gessner & Moller (1971) proposed a shear parameter $S = (\Delta\overline{U}/\overline{U_{cl}})(d/l)$, where $\Delta\overline{U}$ is the velocity change along the length of the wire, and $\overline{U_{cl}}$ is the velocity at the centre of the wire. In the current experiments $S < 2.90 \times 10^{-4}$, and since this is considerably less than the critical value of 10^{-3} suggested by Lomas (1986), errors due to mean shear effects were negligible.

In addition, the wavenumber kl corresponding to the wire length is always greater than about 6300, so that spatial filtering effects should be minor (see § 4.5). Here $k = 2\pi f/U_*$, where f is the frequency and U_* is the local mean velocity.

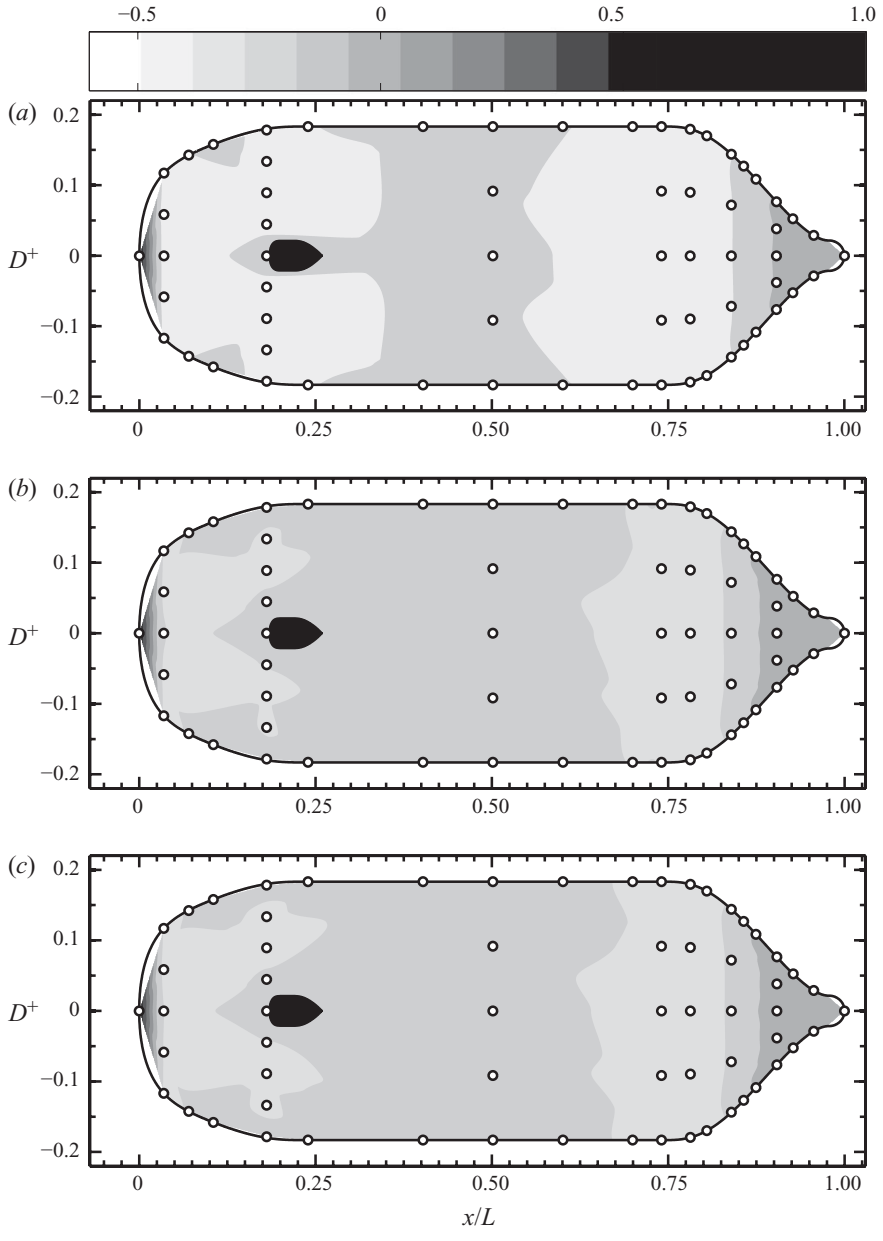

FIGURE 3. Contour maps of the coefficient of pressure based on measurements conducted at 45 different pressure taps (indicated by ○). The model surface is mapped onto a plane, hence the distorted aspect ratio. Note that the bottom boundary is coincident with the top boundary. $Re_L = 1.1 \times 10^6$ (*a*), 12×10^6 (*b*) and 25×10^6 (*c*).

4. Results and discussion

4.1. *Surface pressure*

The pressure distributions along the surface of the submarine model are shown for the three lower Reynolds numbers in figure 3. The coefficient of pressure is defined

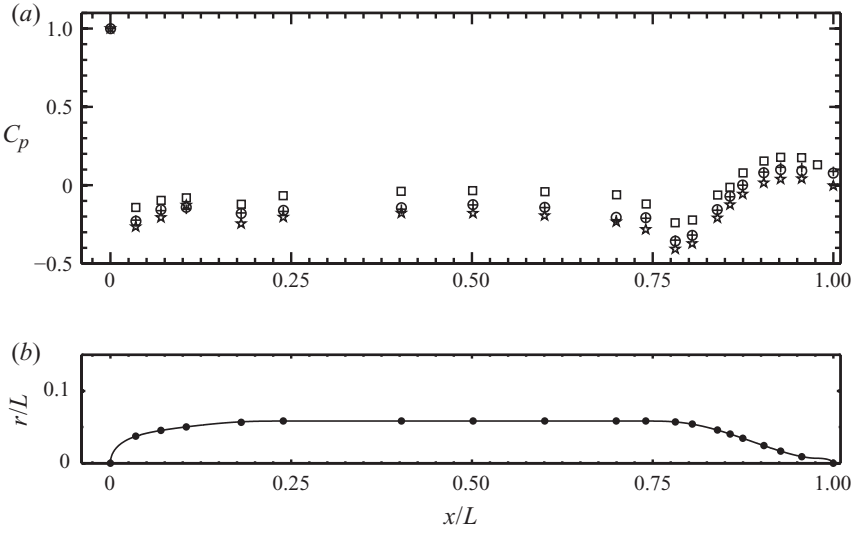

FIGURE 4. (*a*) Coefficient of pressure along the top meridian line of the submarine model on the side opposite the support. ☆, $Re_L = 1.1 \times 10^6$; ○, 12×10^6; +, 25×10^6; □, Huang *et al.* (1992) at $Re_L = 12 \times 10^6$. (*b*) ●, location of pressure taps.

as

$$C_p = \frac{p - p_\infty}{\rho U_\infty^2/2}, \tag{4.1}$$

where p_∞ and $\rho U_\infty^2/2$ are the free-stream static and dynamic pressures, respectively, measured at a point $14.75D$ upstream of the model. The horizontal axis in figure 3 corresponds to the non-dimensional length of the model, x/L, and the vertical axis corresponds to the non-dimensional circumference, $D^+ = \pi D/L$, hence the distorted aspect ratio. The support, located at $x/L \approx 0.2$, also displays a distorted aspect ratio. The bottom boundary is coincident with the top boundary.

In the region $-0.1 < D^+ < 0.1$, the lowest Reynolds number displays a distribution that is significantly different from the higher-Reynolds-number cases. In particular, the pressure is slower to rise over the bow of the model and starts to fall much earlier over the stern, and it demonstrates a much more pronounced effect of the support. For the two higher Reynolds numbers, the distributions are essentially identical given that the contours are constructed from only 45 point measurements. Note that in all cases the downstream effect of the support can be seen clearly in the region $0.6 < x/L < 0.8$. There exist local spanwise bulges in the pressure that are correlated directly with the position of the support, although their influence diminishes rapidly closer to the stern.

The pressure distribution along the top meridian line of the submarine model, which is on the side away from the support and corresponds to the top and bottom boundaries in figure 3, is shown in figure 4. The SUBOFF measurements by Huang *et al.* (1992) at $Re_L = 12 \times 10^6$ follow the same trends as the data presented here, although they appear to be offset by a constant amount. It seems likely that the discrepancy is due to the difference in the reference pressure location. The reference pressure was measured above the model at $x/D \approx -1.3$ for Huang *et al.* (1992), whereas in the present measurements it was obtained at $x/D = -23.3$ ($= 14.75$

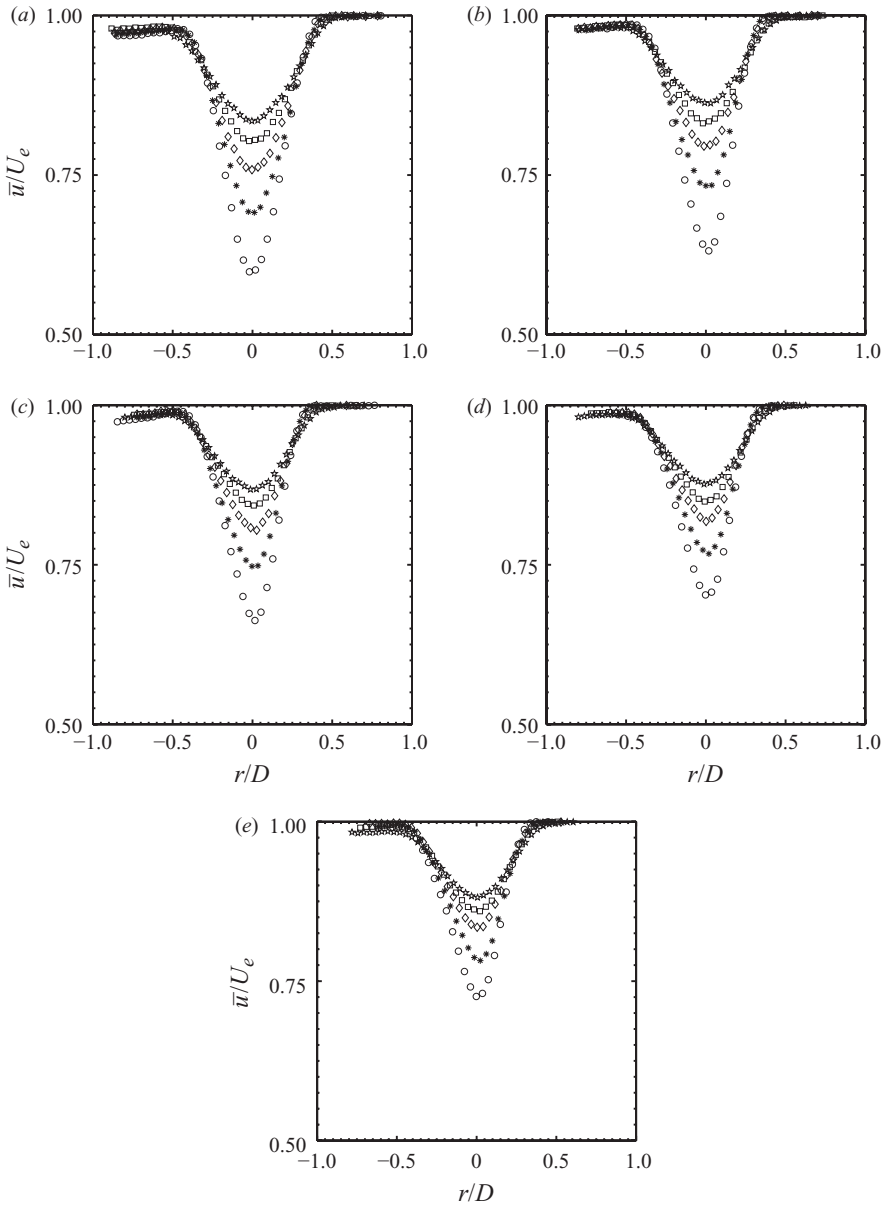

FIGURE 5. Profiles of $\overline{u}/U_e$, at ○, $x/D = 3$; ✳, 6; ◇, 9; □, 12; ☆, 15, for $Re_L = 1.1 \times 10^6$ (*a*), 12×10^6 (*b*), 25×10^6 (*c*), 50×10^6 (*d*) and 67×10^6 (*e*).

upstream of the model nose). In all cases, the pressure is relatively constant over the straight part of the body ($0.23 \leqslant x/L \leqslant 0.74$). The pressure then decreases over the region of convex curvature near the start of the stern taper, before increasing over the region of concave curvature near the end of the stern. The concave portion of the stern has been identified as a region where the boundary-layer thickens rapidly due to a significant static pressure variation across the boundary layer (Patel, Nakayama & Damian 1974; Huang *et al.* 1992).

	Case 1		Case 2	
Re_L	A	B	A	B
1.1×10^6	1.15	0.105	1.18	0.113
12×10^6	1.01	0.091	1.034	0.098
25×10^6	0.93	0.087	0.96	0.094
50×10^6	0.85	0.085	0.875	0.092
67×10^6	0.79	0.084	0.808	0.091
x_0/D	1.80	4.68	2.08	2.08
σ^2	0.00176	0.00067	0.00191	0.00169

TABLE 1. Coefficients in the power-law relationships for u_0 and l_0.

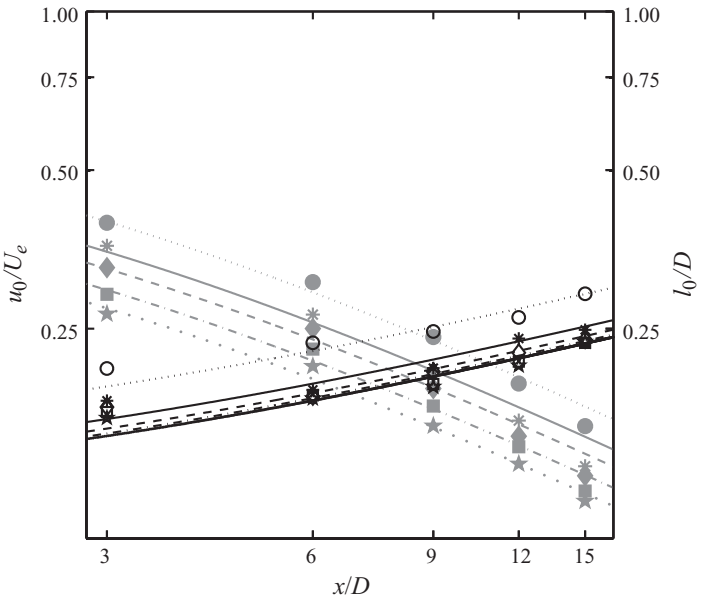

FIGURE 6. Similarity scales for the wake velocity deficit u_0 (grey symbols) and corresponding correlations (grey lines); half-wake width l_0 (black symbols) and corresponding correlations (black lines), for ○, $Re_L = 1.1 \times 10^6$; ✳, 12×10^6; ◇, 25×10^6; □, 50×10^6; ☆, 67×10^6. The values of A, B and x_0 for the correlations correspond to case 2 in table 1.

4.2. *Mean velocity*

Figure 5 shows the mean velocity profiles non-dimensionalized by U_e, the local free-stream velocity, for all Reynolds numbers. The strength of the wake decreases rapidly with downstream distance, and it is clear that the support affects the velocity distributions.

The similarity scales for the defect velocity and half-wake width were found to follow power-law relationships given by $A(x/D + x_0/D)^{-2/3}$ and $B(x/D + x_0/D)^{1/3}$, respectively, as expected from the similarity analysis by Townsend (1956). Various nonlinear curve fits were tried and results are shown in table 1. The most accurate curve fit was attained by minimizing the sum of the squared residuals, σ^2, where the residual is the difference between the measured value and the value provided by the curve fit. For case 1, x_0 was unrestrained for each curve fit and yielded different x_0

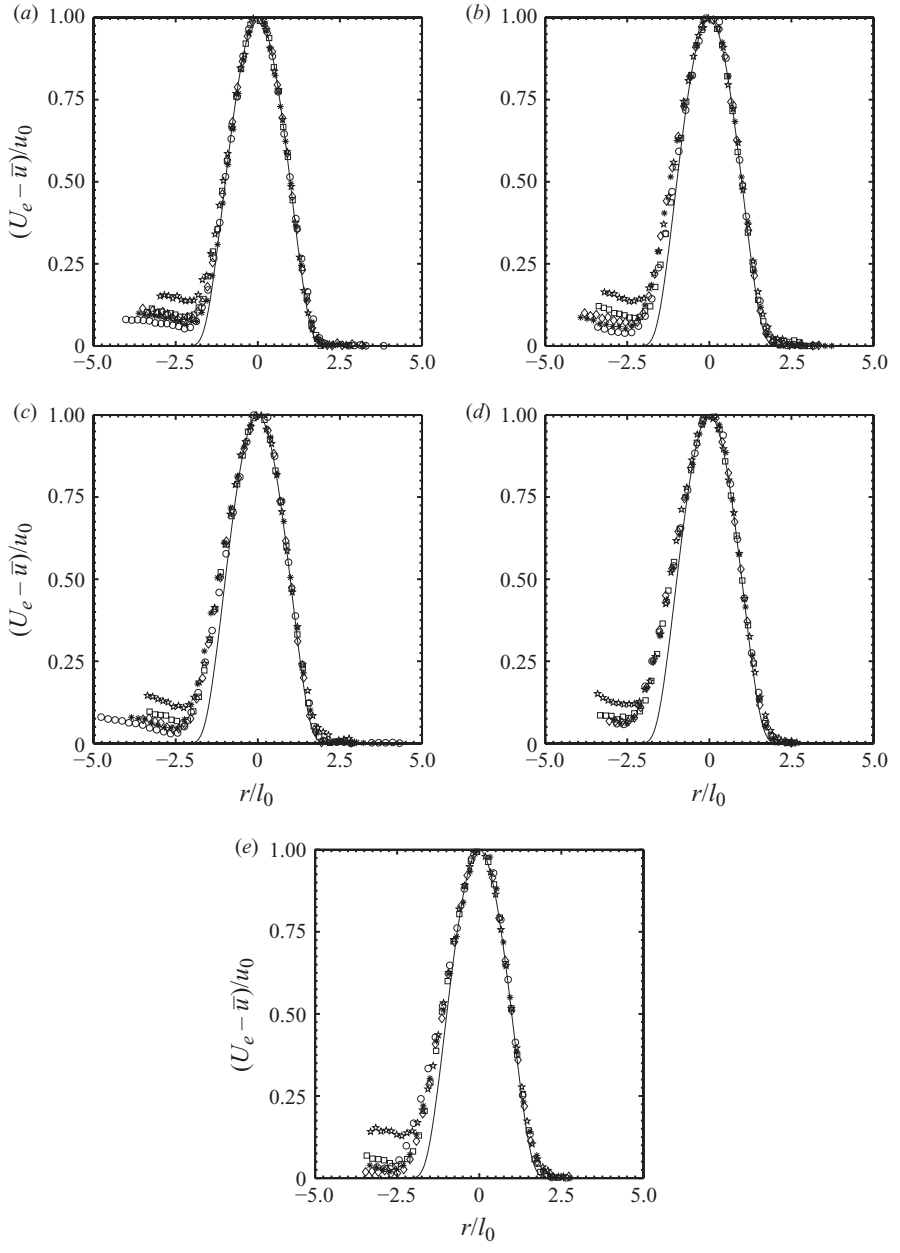

FIGURE 7. Mean velocity in similarity coordinates, for ○, $x/D = 3$; ✳, 6; ◇, 9; □, 12; ☆, 15. Solid line is equation (4.2). $Re_L = 1.1 \times 10^6$ (*a*), 12×10^6 (*b*), 25×10^6 (*c*), 50×10^6 (*d*) and 67×10^6 (*e*).

values for the defect velocity and half-wake width relationships. For case 2, x_0 was unrestrained for each curve fit, but forced to be equal for the defect velocity and half-wake width. Case 1 yielded lower values of σ^2, but the values of A and B do not depend strongly on the virtual origin position, and they appear to asymptote towards constant values at high Reynolds numbers. This indicates that the wake is still evolving slowly in the streamwise direction over this range of x/D locations. The

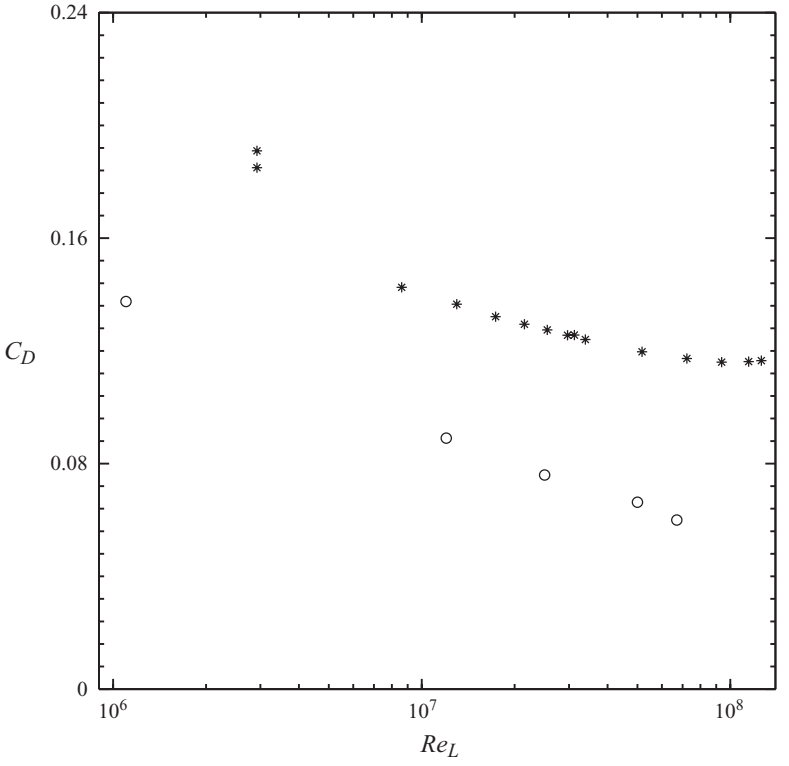

FIGURE 8. Coefficients of drag. ○, SUBOFF model; ✳, DTMB 5495-3 model with a conical stern by Bridges, Cash & Freudenthal (2006).

values for A, B and x_0 for the power-law relationships shown in figure 6 correspond to case 2. Jiménez *et al.* (2010) found that $A = 1.053$ and $B = 0.110$ at $Re_L = 1.1 \times 10^6$, which are slightly different to the values found here at the same Reynolds number, probably because Jiménez *et al.* (2010) determined A and B from data taken over a shorter streamwise distance ($3 \leqslant x/D \leqslant 9$).

Symes & Fink (1977) observed that for the wakes of circular cylinders an increase in free-stream turbulence intensity leads to larger half-wake widths, smaller velocity deficits and an earlier attainment of self-similarity. Although the free-stream turbulence intensity in the HRTF increases with Reynolds number from a minimum of 0.3 % to a maximum of 1.1 %, there is no obvious influence on the wake development. The velocity deficits are larger for the $Re_L = 1.1 \times 10^6$ case (figure 6). This is probably a low-Reynolds-number effect, since low-Reynolds-number boundary layers are more susceptible to adverse pressure gradients, resulting in a wider wake, as seen in figure 6 where the half-wake width is consistently larger for $Re_L = 1.1 \times 10^6$ compared to the higher Reynolds numbers.

Figure 7 shows the mean velocity distributions in similarity coordinates, which highlights the effects of the support already seen in figure 5. This asymmetry has also been observed in the velocity profiles downstream of the sail in SUBOFF numerical simulations at $Re_L = 12 \times 10^6$ by Alin *et al.* (2000), and experimentally by Jiménez *et al.* (2010) at $Re_L = 1.1 \times 10^6$. On the side away from the support ($r/l_0 > 0$), however, the distributions show a self-similar behaviour at all downstream locations and at all Reynolds numbers. The profile on this side is accurately described by the

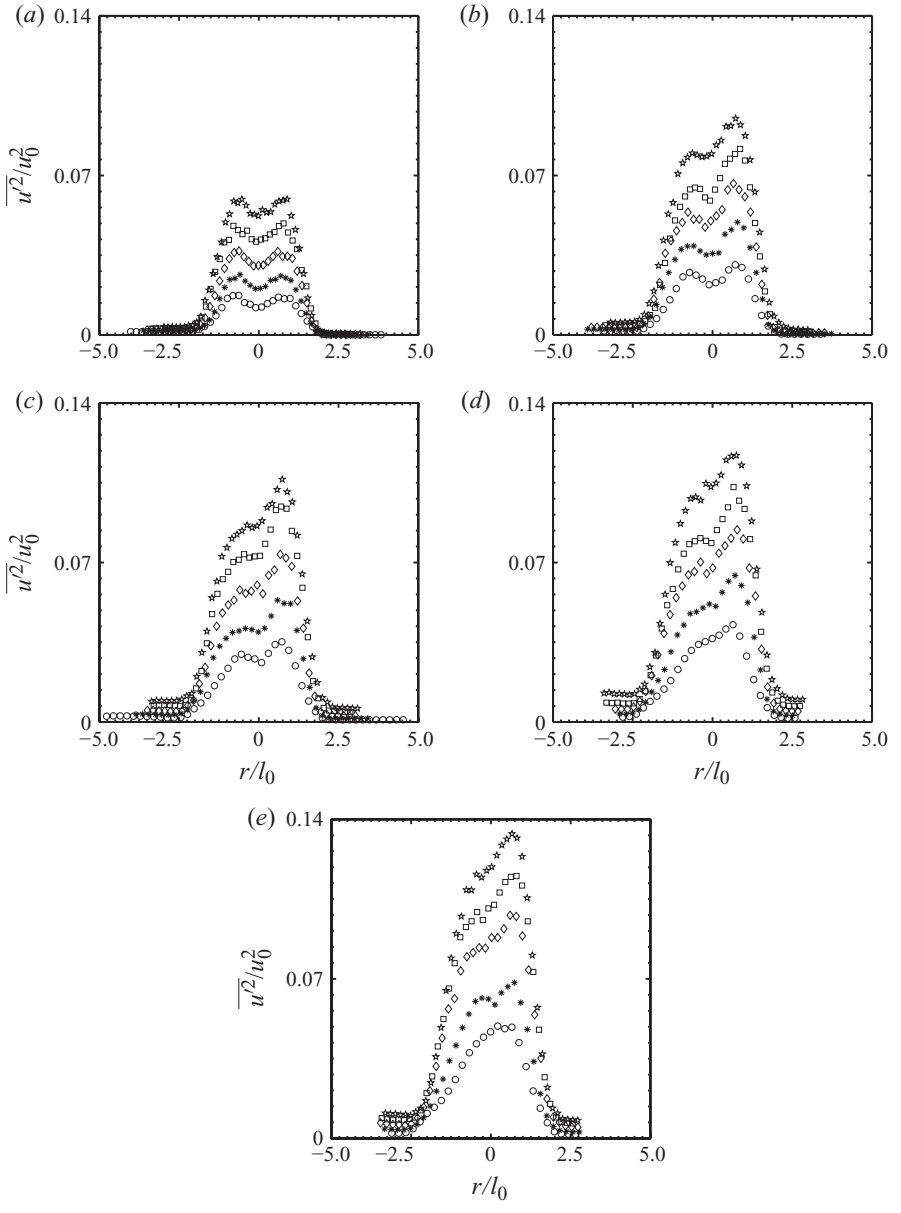

FIGURE 9. Variance of the streamwise velocity fluctuations in similarity coordinates for ○, $x/D = 3$; ✳, 6; ◇, 9; □, 12; ☆, 15, for $Re_L = 1.1 \times 10^6$ (*a*), 12×10^6 (*b*), 25×10^6 (*c*) (d) 50×10^6 (*d*) and 67×10^6 (*e*).

function:

$$f(\eta) = \exp(-0.61\eta^2 - 0.065\eta^4 - 0.03\eta^6 - 0.006\eta^8). \tag{4.2}$$

A similar function was reported by Jiménez *et al.* (2010) at lower Reynolds numbers, with slightly different values of the coefficients. Equation (4.2) also describes the velocity profile on the side with the support, at least for $r/l_0 \geqslant -1$, but further from the centreline the effect of the support is to reduce the velocity gradients. The mean velocity displays self-similarity as early as $x/D = 3$. This is consistent with the

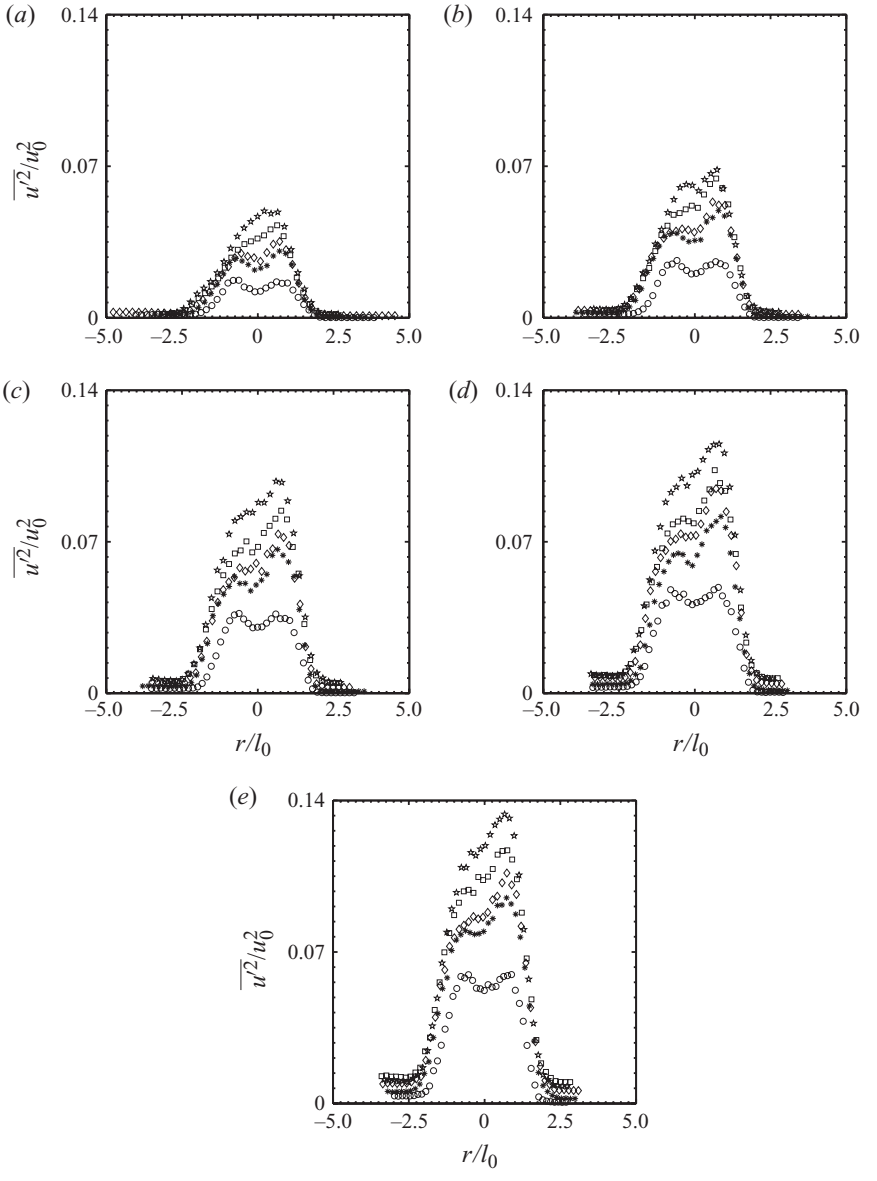

FIGURE 10. Variance of the streamwise velocity fluctuations in similarity coordinates for ○, $Re_L = 1.1 \times 10^6$; ✳, 12×10^6; ◇, 25×10^6; □, 50×10^6; ☆, 67×10^6, at $x/D = 3$ (*a*), 6 (*b*), 9 (*c*), 12 (*d*) and 15 (*e*).

results of Chevray (1968) in the wake of a prolate spheroid at $Re_L = 2.75 \times 10^6$ and in axisymmetric wakes over a broad range of axial positions at very low Reynolds numbers (Higuchi & Kubota 1990).

The coefficient of drag may be calculated from the wake mean-velocity distribution, using the methods outlined by Dimotakis (1977) and Bridges *et al.* (2006). The contributions from the gradients of pressure and normal stresses are negligible for $x/D \geqslant 3$. It was assumed that (4.2) holds for the entire wake in order to find the drag coefficient of the unsupported body. The results are shown in

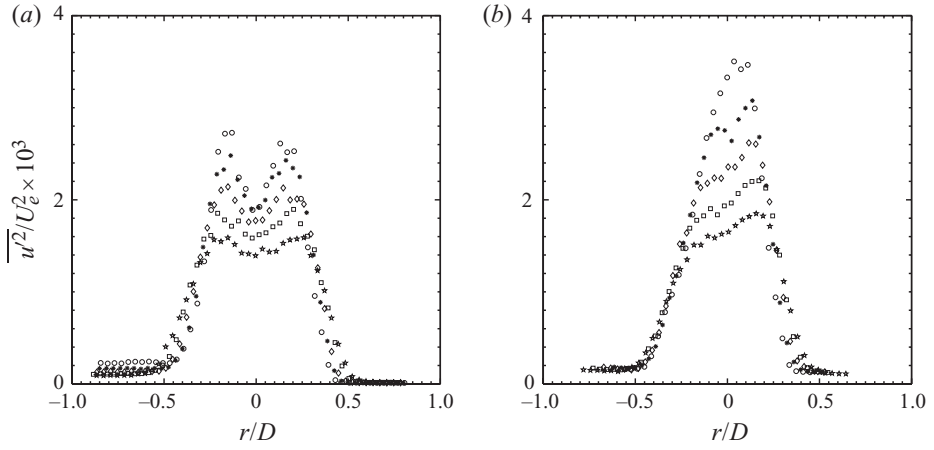

FIGURE 11. Distributions of the mean square turbulence intensity at ○, $x/D = 3$; ✳, 6; ◇, 9; □, 12; ☆, 15 for $Re_L = 1.1 \times 10^6$ (*a*) and 67×10^6 (*b*).

figure 8, where they are compared with the data from Bridges *et al.* (2006) for an axisymmetric submarine model with a conical stern (DTMB model 5495-3). Although broadly similar trends are observed, the SUBOFF drag coefficients are significantly lower. Also, the DTMB data appear to show the effects of roughness for $Re_L > 80 \times 10^6$, in that the drag coefficient is becoming independent of Reynolds number.

4.3. *Turbulence*

Figures 9 and 10 show the variance of the streamwise velocity fluctuations in similarity coordinates. Unlike the mean velocity, the turbulence shows no evidence of self-similarity at any Reynolds number or downstream location. For all Reynolds numbers, the levels increase with increasing x/D since $\overline{u'^2}$ decreases more slowly than u_0^2 (figure 9). A similar behaviour is seen with increasing Reynolds number at a fixed x/D (figure 10). Figure 11 shows the mean square turbulence intensity $\overline{u'^2}/U_e^2$ versus r/D at the two extreme Reynolds numbers, demonstrating that, as expected, the turbulence intensity decreases with increasing downstream distance but, as seen from figure 9, it does not decrease as rapidly as u_0^2.

For the lowest Reynolds number, the turbulence profiles are relatively symmetric at all downstream locations, displaying a local minimum on the centreline and two distinct peaks at $r/l_0 \approx \pm 1 (r/D \approx \pm 0.15)$. The shape of this bimodal distribution has its origin in the development of the boundary layer near the stern, where the thin boundary layer over the constant diameter zero-pressure-gradient region transitions to a thicker profile in the adverse pressure gradient tail region. This change in pressure gradient causes the turbulence intensity values to decrease near the wall so that the location of the maximum value shifts away from the wall (Patel *et al.* 1974; Merz *et al.* 1985). This behaviour is as expected, demonstrating the formation of the wake as a merging of the axisymmetric boundary layer, reflecting the distribution of large vortical structures about the centreline (Sato & Kuriki 1961; Ramaprian & Patel 1982; Wygnanski *et al.* 1986). Johansson & George (2006*a*) found that for a circular disk the twin peaks were a feature of the entire wake, persisting into the far (self-similar) wake.

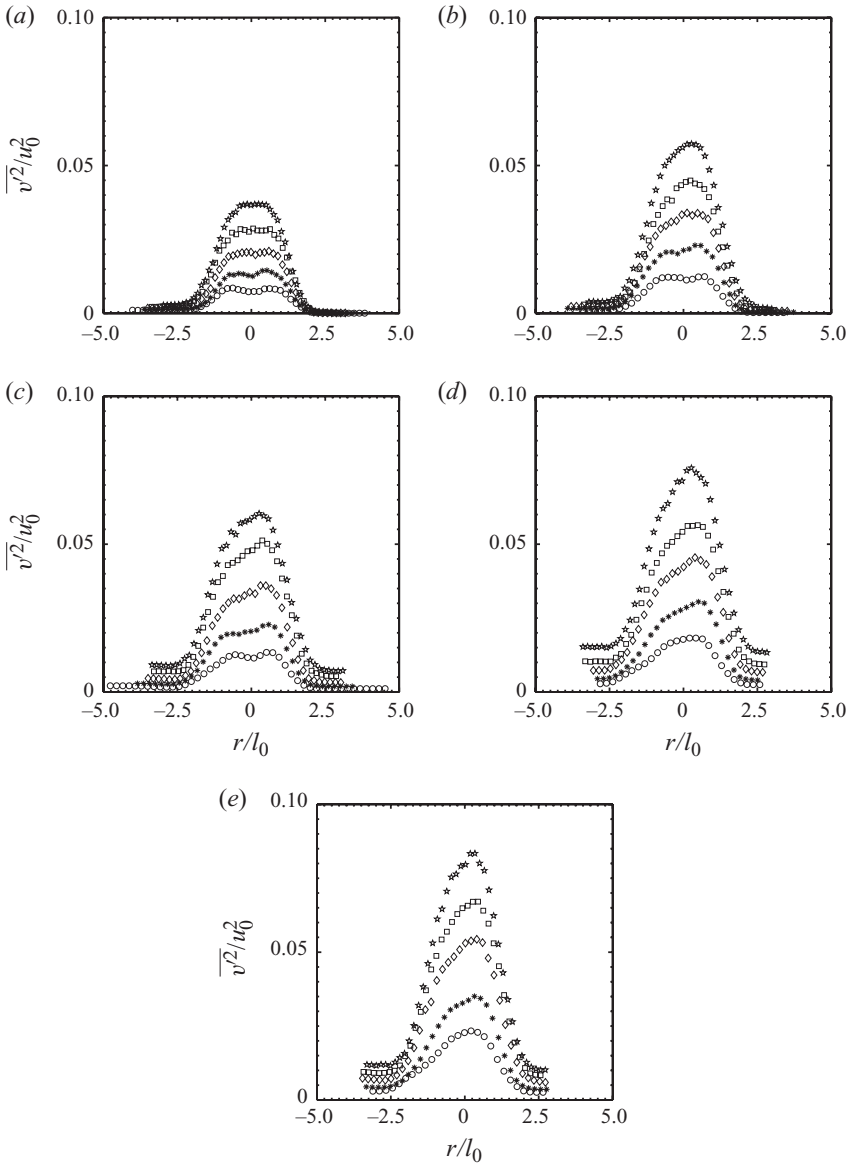

FIGURE 12. Variance of the radial velocity fluctuations in similarity coordinates at ○, $x/D = 3$; ✳, 6; ◇, 9; □, 12; ☆, 15 for $Re_L = 1.1 \times 10^6$ (*a*), 12×10^6 (*b*), 25×10^6 (*c*) 50×10^6 (*d*) and 67×10^6 (*e*).

For the SUBOFF wake at higher Reynolds numbers, however, the profiles become distinctly asymmetric, and the asymmetry increases with Reynolds number and downstream position. In all cases, the larger peak appears on the non-support side ($r/D > 0$), but at sufficiently high Reynolds number the peak on the support side disappears entirely, exaggerating the level of asymmetry and reflecting the strong influence of the support on the evolution of the wake below the centreline.

The radial turbulence fluctuations display similar trends to those seen for the streamwise component (see figure 12). Again, there is no clear indication that the

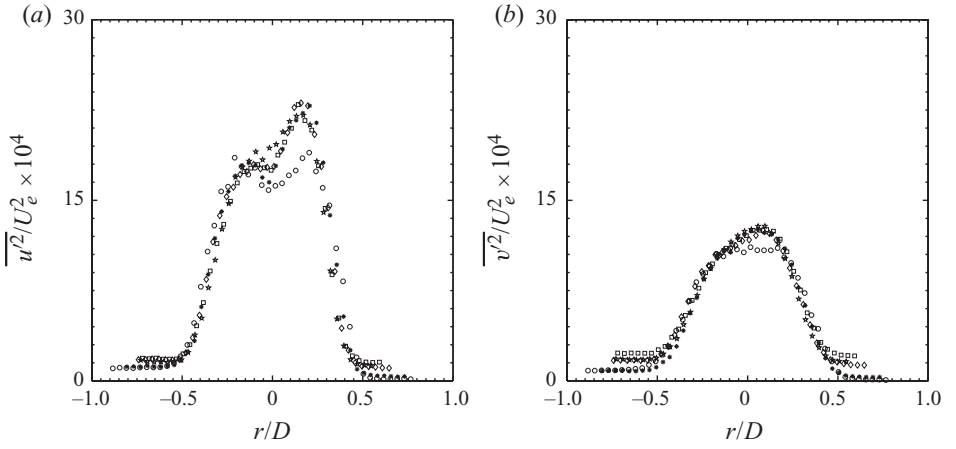

FIGURE 13. Distributions of the mean square turbulence intensities at $x/D = 12$ for ○, $Re_L = 1.1 \times 10^6$; ✳, 12×10^6; ◇, 25×10^6; □, 50×10^6; ☆, 67×10^6. (*a*) Streamwise component; (*b*) radial component.

profiles are approaching a self-similar state, although the influence of the support seems less marked in that the strong asymmetry seen in the streamwise component is not as evident in the radial component. This may suggest that the orientation of fluid structures is becoming more random as it transitions from the configuration present in a turbulent boundary layer to a more homogeneous free shear flow.

It should be noted that the focus on similarity scaling tends to mask the behaviour of the turbulence itself. At any fixed downstream location, the streamwise and radial turbulence intensities are almost independent of Reynolds number for all but the lowest Reynolds number. This is shown in figure 13 for $x/D = 12$, which is representative of the behaviour at other downstream locations. It appears that similarity scales are not particularly useful for describing the turbulence in the intermediate wake, and we see that in absolute terms effects of Reynolds number variations on the turbulence are small for $Re_L \geqslant 12 \times 10^6$.

The turbulent shear stress results are plotted in figure 14. As seen for the normal stresses, the distribution is relatively symmetric for $Re_L = 1.1 \times 10^6$, but asymmetric for the larger Reynolds numbers, with larger magnitudes on the side without the support. The distributions have not attained self-similarity for any of the locations or Reynolds numbers studied, but the effects of Reynolds number are less pronounced than for the normal stresses, even in similarity coordinates.

The maximum values of the Reynolds stresses, $\overline{u_m'^2}/u_0^2$, $\overline{v_m'^2}/u_0^2$ and $\overline{u'v'_m}/u_0^2$, are shown in figure 15 for the side away from the support. The figure summarizes the trend to self-similarity. There exists only a weak Reynolds number dependence (excluding the lowest Reynolds number), and all components display a reduced growth rate for $x/D > 9$, although it is apparent that self-similarity will not be attained in the intermediate wake. It may well take as long as that observed by Johansson & George (2006*a*) in the wake behind a circular disk, where they found that the intermediate wake extended to $x/D = 30$.

4.4. *Local effects of the support*

An important question is whether the flow opposite the support is representative of the unsupported wake, that is, one that is free of any support interference. To answer

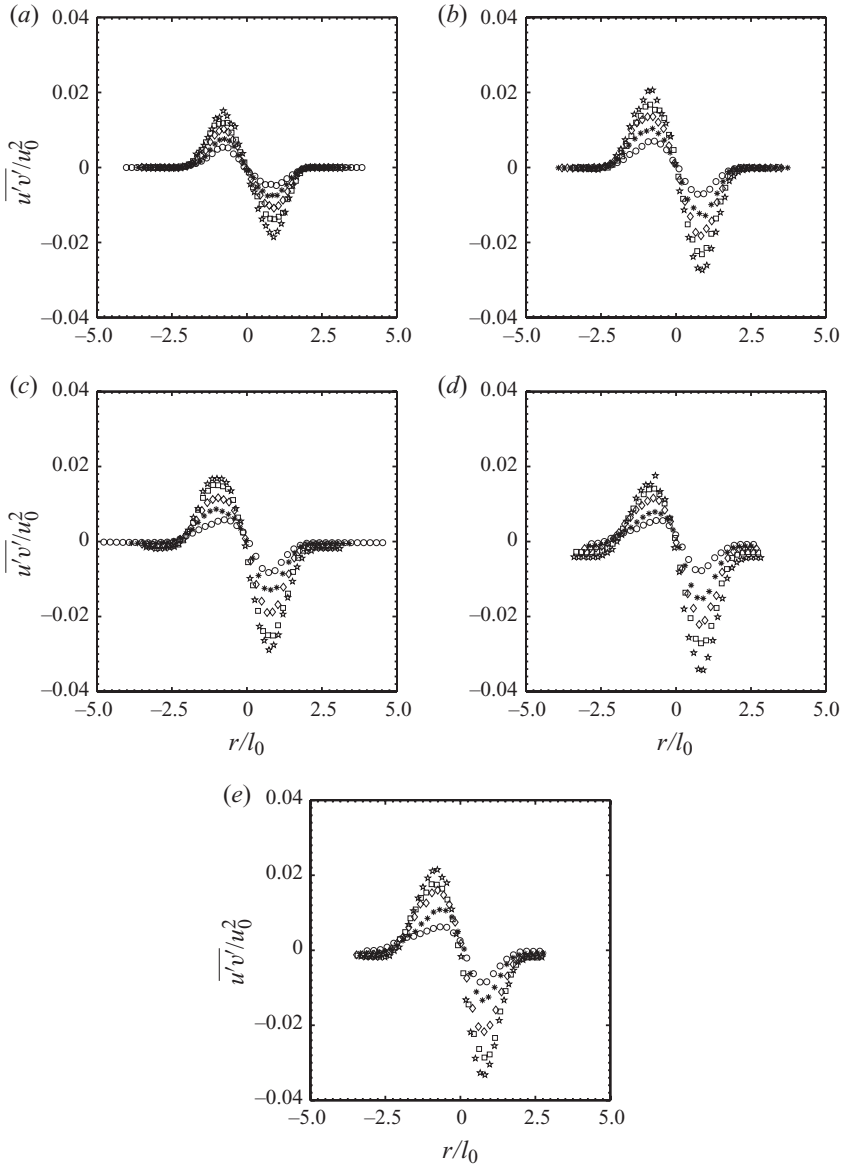

FIGURE 14. Turbulent shear stress in similarity coordinates at: ○, $x/D = 3$; ✳, 6; ◇, 9; □, 12; ☆, 15 for $Re_L = 1.1 \times 10^6$ (*a*); 12×10^6 (*b*); 25×10^6 (*c*); 50×10^6 (*d*); 67×10^6 (*e*).

this question, additional measurements were conducted in the horizontal and vertical planes at $x/D = 12$ for $Re_L = 25 \times 10^6$. Due to the limitations of the traversing system, the centres of these planes were displaced by about 2 mm towards the support side, resulting in small differences in the magnitudes of the fluctuations compared to the main body of the data presented here. Figure 16 demonstrates that for $r/l_0 > 0$ the results for both planes agree in the mean velocity and in the fluctuation levels within the experimental uncertainty, confirming that the support affects only the lower side of the wake $r/l_0 < 0$, where it attenuates the fluctuation levels and decreases the mean velocity.

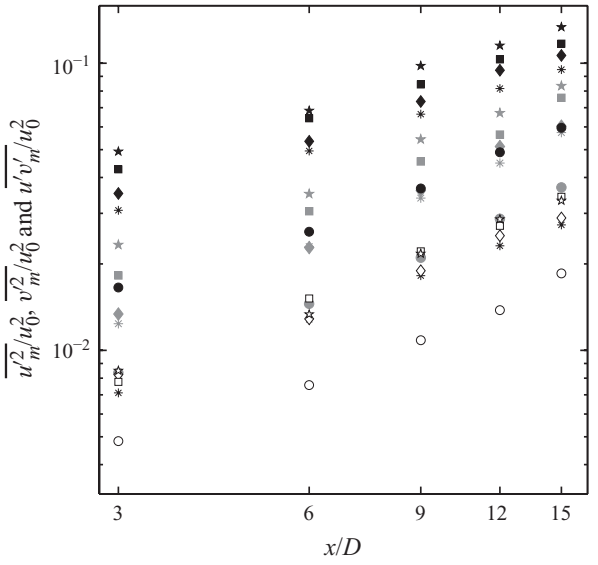

FIGURE 15. Reynolds stress maxima, $\overline{u_m'^2}/u_0^2$ (black solid symbols), $\overline{v_m'^2}/u_0^2$ (grey solid symbols) and $\overline{u'v_m'}/u_0^2$ (black hollow symbols) for ○, $Re_L = 1.1 \times 10^6$; ✳, 12×10^6; ◇, 25×10^6; □, 50×10^6; ☆, 67×10^6.

4.5. *Energy spectra*

To examine the frequency content of the turbulence, the pre-multiplied energy spectra $k\Phi_{uu}$ are shown in figures 17 and 18. A striking feature is seen for $Re_L \geqslant 12 \times 10^6$, where a low-wavenumber peak is present at $kl_0 \approx 0.3$, corresponding to a Strouhal number $St = fD/U_\infty \approx 0.2$. This peak may indicate the presence of a coherent shedding process in the wake. The peak is observed at all radial locations in the streamwise component (figure 18), although it weakens as x/D and r/D increase. This feature is not seen in the energy spectra for the radial component (data not shown). The low-wavenumber peak appears at $Re_L = 12 \times 10^6$, which is the same value where the turbulence intensity profiles become asymmetric, suggesting a causal connection. Figures 18(c) and 18(d) show that this peak, even if weaker downstream, is still present at $x/D = 15$. Self-similarity is not expected to occur until this memory of the wake generator has disappeared.

5. Discussion and conclusions

Experiments over an unprecedented Reynolds number range from $Re_L = 1.1 \times 10^6$ to 67×10^6 have revealed the characteristics of the intermediate wake generated by an axisymmetric body based on the DARPA SUBOFF geometry. The model was mounted on one side by a support formed by an extension of the sail, and the support introduced a strong asymmetry in the wake at all but the lowest Reynolds number.

On the side away from the support, the mean velocity profiles collapsed in similarity scaling at all locations and Reynolds numbers. This scaling also described the velocity profile on the side with the support, at least for $r/l_0 \geqslant -1.0$, but for larger distances from the centreline the support reduced the velocity gradients in the wake.

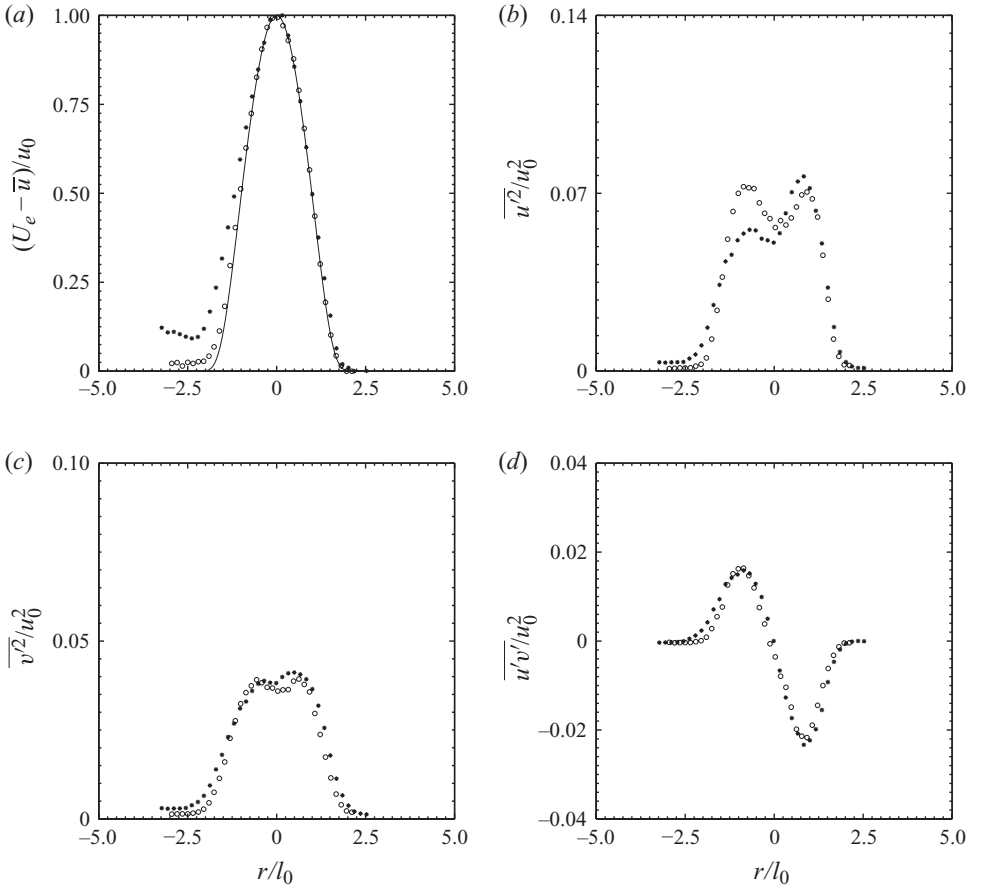

FIGURE 16. Horizontal, ○, and vertical, ✳, plane wake measurement comparisons at $x/D = 12$ and $Re_L = 25 \times 10^6$ demonstrate the effects of the support. Distributions in similarity coordinates of the (*a*) mean velocity with solid line corresponding to (4.2), (*b*) variance of the axial velocity fluctuations, (*c*) variance of the radial velocity fluctuations and (*d*) turbulent shear stress.

The streamwise and radial turbulence intensity values, as well as the Reynolds shear stresses, were still far from self-similar at the furthest downstream location, but the data showed a tendency to self-similarity for $x/D > 9$ on the side away from the support, at a rate similar to that seen in the wake of a circular cylinder by Johansson & George (2006*a*). At the lowest Reynolds number the profiles were approximately symmetric with twin peaks of similar magnitude on either side of the centreline, but at higher Reynolds numbers the peak on the side of the support disappeared, and all the Reynolds stresses on that side were lower than the levels seen on the side away from the support. The anisotropy decreased with downstream distance where $\overline{u'^2}/\overline{v'^2}$ was about 2 at $x/D = 3$ for all Reynolds numbers, but at $x/D = 15$ this ratio had decreased to about 1.3.

The spectra revealed a peak at a Strouhal number of about 0.2 for all the higher Reynolds numbers, suggesting the presence of a coherent shedding process. The peak was evident on both sides of the wake, but reduced sharply with increasing distance

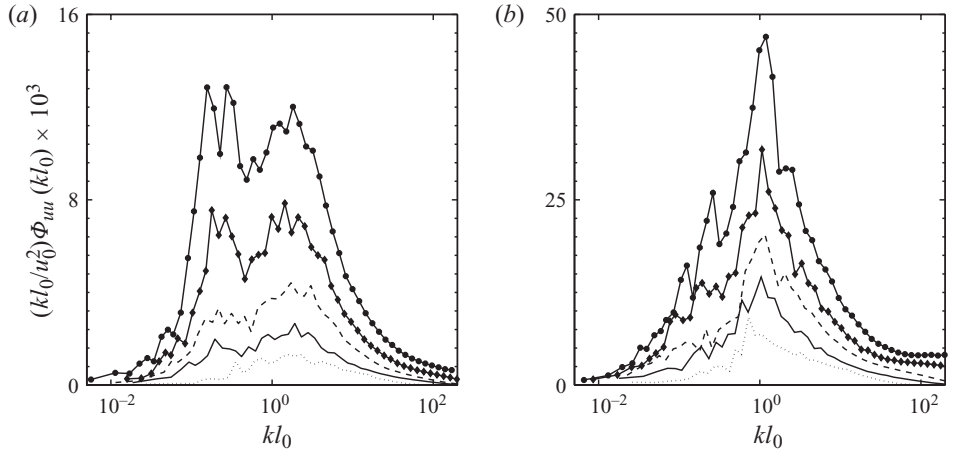

FIGURE 17. Energy spectra of the streamwise velocity component at $r/l_0 = 0$ for $\cdots$, $Re_L = 1.1 \times 10^6$; ——, 12×10^6; – – –, 25×10^6 ; —◆—, 50×10^6; —●—, 67×10^6. (*a*) $x/D = 3$; (*b*) 15.

downstream. The slow decay of vortices shed into the wake may well be a contributing factor in setting the rate at which the wake approaches self-similarity.

The lowest Reynolds number wake behaves very differently from the higher Reynolds number cases. At the lowest Reynolds number the pressure distribution shows a markedly greater influence of the support, the wake is almost exactly symmetric and there is no evidence for the shedding of coherent structures into the wake. In many respects, the low-Reynolds-number wake is what would be expected from the wake generated by a body of revolution, in the absence of the effects of a support. Three aspects, however, may come into play at this Reynolds number: (i) the trip wire may not be fully effective, (ii) the flow over the stern may separate earlier and (iii) the support boundary layer is most likely laminar, since the chord Reynolds number is only 9.3×10^4. With respect to the first aspect, Jiménez *et al.* (2010) in a related study on the effects of fins on the wake found that the trip appeared to be fully effective, even at this Reynolds number. Also, in earlier work in the HRTF, the model wake was examined in the absence of the trip wire, and the mean velocity profiles at this Reynolds number were quite different from those reported here. Regarding the second aspect, although the boundary layer may be expected to separate earlier at lower Reynolds numbers, there is little evidence in the pressure distributions near the stern to support this possibility. With reference to the third aspect, even if the support boundary layer is laminar its wake will quickly transition to turbulence and would not be expected to show any significant Reynolds number effects far downstream. At this point there appears to be no obvious explanation for the apparently anomalous behaviour at the lowest Reynolds number.

Considering the higher Reynolds numbers, for $Re_L \geqslant 12 \times 10^6$ the variation of the absolute turbulence levels with Reynolds number is probably negligible within the experimental uncertainty, and similarity scaling is not appropriate. The approach to self-similarity was certainly slow, and appeared to be similar to that seen by Johansson & George (2006*a*) in the wake behind a circular disk, where they found that the intermediate wake extended to $x/D = 30$. The dominant parameter is the downstream development length, and not the Reynolds number.

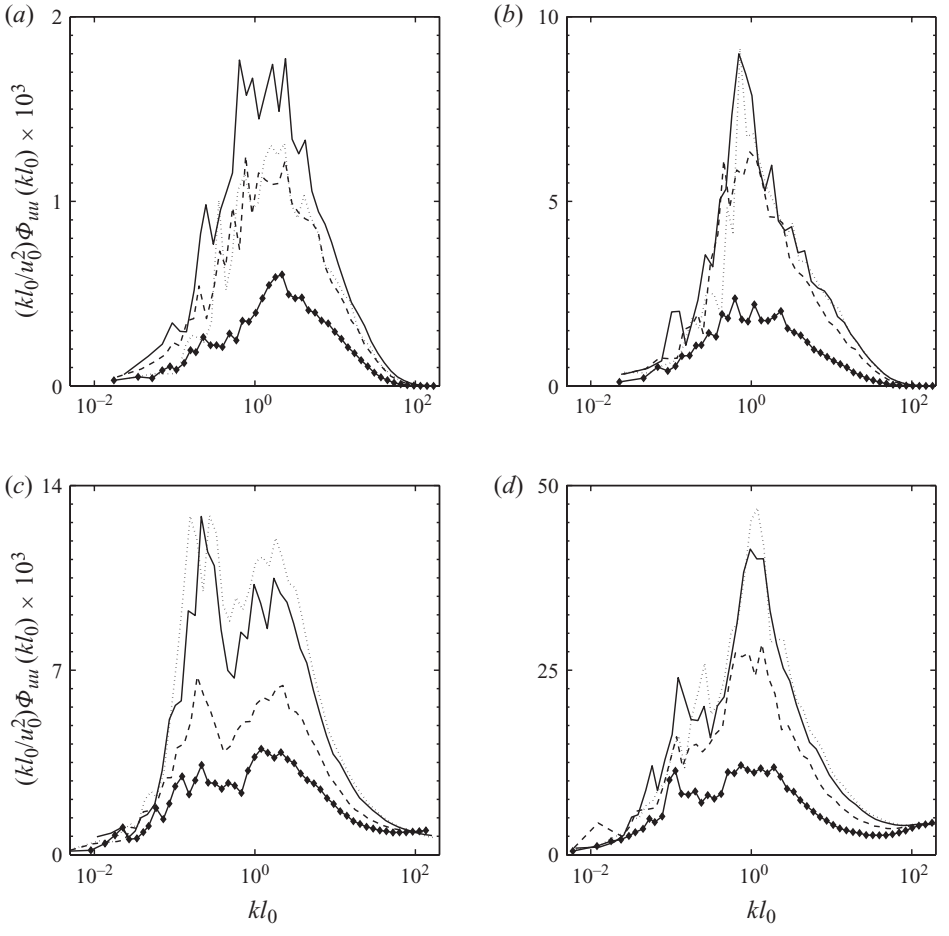

FIGURE 18. Energy spectra of the streamwise velocity component at $\cdots$, $r/l_0 = 0.0$; ——, 0.5; – – –, 1.0; —◆—, 1.5; for: (*a*) $Re_L = 1.1 \times 10^6$ at $x/D = 3$, (*b*) $Re_L = 1.1 \times 10^6$ at $x/D = 15$, (*c*) $Re_L = 67 \times 10^6$ at $x/D = 3$, (*d*) $Re_L = 67 \times 10^6$ at $x/D = 15$.

It was found that the wake on the side away from the support is not influenced by the support wake, or by the flow produced in the support/body junction. For the flow in the plane of the support, the mean velocity profiles suggest that the effects of the support are confined to a region $r/l_0 < -1$, whereas the turbulence profiles are affected for $r/l_0 < 0$. The effects of the support on the wake development appear to be similar to the effects introduced by the sail on a submarine wake. The support/junction flow is expected to be similar to the sail/hull junction flow, but the aspect ratio of the support is obviously much larger than that for the sail, and so the tip vortex is not present. However, both the tip vortex and junction vortices are weak at zero yaw angle (Jiménez 2007), and the dominant influence seems to be the interference that occurs between the wake generated by the support and the wake generated by the body of revolution. The result is to decrease all the Reynolds stresses on the support side.

This work was made possible by support received under ONR Grants N00014-03-1-0320, N00014-07-1-0111 and N00014-09-1-0263, monitored by Dr Ron Joslin.

REFERENCES

Alin, N., Berglund, M. & Fureby, C. 2000 A VLES approach applied to flows around underwater vehicle hulls. In *Thirty-eighth AIAA Aerospace Sciences Meeting and Exhibit*. Reno, NV.

Arabshahi, A., Beddhu, M., Briley, W., Chen, J., Gaither, A., Gaither, K., Janus, J., Jiang, M., Marcum, D., McGinley, J., Pankajakshan, R., Remotigue, M., Sheng, C., Sreenivas, K., Taylor, L. & Whitfield, D. 1998 A perspective on naval hydrodynamics flow simulations. In *Twenty-second Symposium on Naval Hydrodynamics*. Washington, DC.

Bradshaw, P. B. 1971 *An Introduction to Turbulence and its Measurement*. Pergamon Press.

Bridges, D. H., Cash, A. C. & Freudenthal, J. L. 2006 Investigation of scaling effects in submarine flows. In *Forty-fourth AIAA Aerospace Sciences Meeting and Exhibit*. Reno, NV.

Bull, P. 1996 The validation of CFD predictions of nominal wake for the SUBOFF fully appended geometry. In *Twenty-first Symposium on Naval Hydrodynamics*. Trondheim, Norway.

Carmody, T. 1964 Establishment of the wake behind a disk. *J. Basic Engng* **87**, 869–882.

Chevray, R. 1968 The turbulent wake of a body of revolution. *J. Basic Engng* **90**, 275–284.

Desabrais, K. J. & Johari, Hamid 2006 Vortex shedding in the near wake of rigid and flexible bluff bodies. In *Forty-fourth AIAA Aerospace Sciences Meeting and Exhibit*. Reno, NV.

Dimotakis, P. E. 1977 Laser Doppler velocimetry momentum defect measurements of cable drag at low to moderate Reynolds numbers. *Tech. Rep.* N62583/77-M-R541. NCBC.

Gear, P. J. L. 1965 An experimental study of the turbulence in the wake of a body of revolution. Master's thesis, University of Iowa, Iowa City, IA.

Gessner, F. B. & Moller, G. L. 1971 Response behaviour of hot wires in shear flow. *J. Fluid Mech.* **47**, 449–468.

Goldstein, S. 1948 Low-drag and suction airfoils. *J. Aeronaut. Sci.* **15**, 189–220.

Groves, N. C., Huang, T. T. & Chang, M. S. 1989 Geometric characteristics of DARPA SUBOFF models. *Tech. Rep.* DTRC/SHD-1298-01. David Taylor Research Center, Bethesda, MD.

Higuchi, H. & Kubota, T. 1990 Axisymmetryc wakes behind a slender body including zero-momentum configurations. *Phys. Fluids* A **2** (9), 1615–1623.

Hosder, S. 2001 Unsteady skin-friction measurements on a maneuvering DARPA2 SUBOFF model. Master's thesis, Virginia Polytechnic Institute and State University, Blacksburg, VA.

Huang, T., Liu, H. L., Groves, N., Forlini, T., Blanton, J. & Gowing, S. 1992 Measurements of flows over an axisymmetric body with various appendages in a wind tunnel: the DARPA SUBOFF experimental program. In *Nineteenth Symposium on Naval Hydrodynamics*. Seoul, Korea.

Hultmark, M. & Smits, A. J. 2010 A note on temperature corrections for hot wires. *Meas. Sci. Technol.* (in press).

Jiménez, J. M. 2007 High Reynolds number flows about bodies of revolution with application to submarines and torpedoes. PhD thesis, Princeton University, Princeton, NJ.

Jiménez, J. M., Reynolds, R. & Smits, A. J. 2010 The effects of fins on the intermediate wake of a submarine model. *J. Fluids Engng* **132** (3), 031102.

Johansson, P. B. V. & George, W. K. 2006*a* The far downstream evolution of the high-Reynolds-number axisymmetric wake behind a disk. Part 1. Single-point statistics. *J. Fluid Mech.* **555**, 363–385.

Johansson, P. B. V. & George, W. K. 2006*b* The far downstream evolution of the high-Reynolds-number axisymmetric wake behind a disk. Part 2. Slice proper orthogonal decomposition. *J. Fluid Mech.* **555**, 387–408.

Lomas, C. G. 1986 *Fundamentals of Hot-wire Anemometry*. Cambridge University Press.

McDonald, H. & Whitfield, D. 1996 Self-propelled maneuvering underwater vehicles. In *Twenty-first Symposium on Naval Hydrodynamics*. Trondheim, Norway.

Merz, R. A., Yi, C. H. & Przirembel, C. E. G. 1985 The subsonic near-wake of an axisymmetric semielliptical afterbody. *AIAA J.* **23** (10), 1512–1517.

Oertel, H. 1990 Wakes behind blunt bodies. *Annu. Rev. Fluid Mech.* **22**, 539–564.

Patel, V. C., Nakayama, A. & Damian, R. 1974 Measurements in the thick axisymmetric turbulent boundary layer near the tail of a body of revolution. *J. Fluid Mech.* **63**, 345–367.

Perry, A. E. 1982 *Hot-Wire Anemometry*. Oxford University Press.

Ramaprian, B. R. & Patel, V. C. 1982 The symmetric turbulent wake of a flat plate. *AIAA J.* **20**, 1228–1235.

Sato, H. & Kuriki, K. 1961 The mechanism of transition in the wake of a thin flat plate placed parallel to a uniform flow. *J. Fluid Mech.* **11**, 321–352.

Sheng, C., Taylor, L. K. & Whitfield, D. L. 1995 Multiblock multigrid solution of three dimensional incompressible turbulent flows about appended submarine configurations. In *AIAA 33rd Aerospace Sciences Meeting and Exhibit*. Reno, NV.

Simpson, R. L. 2001 Junction flows. *Annu. Rev. Fluid Mech.* **33**, 415–443.

Sirviente, A. I. & Patel, V. C. 1999 Experiments in the turbulent near wake of an axisymmetric body. *AIAA J.* **37** (12), 1670–1672.

Sung, C. H., Griffin, M. J., Tsai, J. F. & Huang, T. T. 1993 Incompressible flow computation of forces and moments on bodies of revolution at incidence. In *AIAA 31st Aerospace Sciences Meeting and Exhibit*. Reno, NV.

Symes, C. R. & Fink, L. E. 1977 Effects of external turbulence upon the flow past cylinders. In *Structures and Mechanisms of Turbulence I* (ed. J. Ehlers, K. Hepp, R. Kippenhahn & H. A. Weidenmüller), pp. 86–102. Berlin, Germany.

Townsend, A. A. 1956 *The Structure of Turbulent Shear Flow*. Cambridge University Press.

Wygnanski, I., Champagne, F. & Marasli, B. 1986 On the large scale structures in two dimensional, small deficit turbulent wakes. *J. Fluid Mech.* **168**, 31–71.

Yavuzkurt, S. 1984 A guide to uncertainty analysis of hot-wire data. *J. Fluids Engng* **106**, 181–186.